RESEARCH ARTICLE

Harnessing the Jahn-Teller Effect for Enhanced Nonlinear Optical Properties in Nano-magnetic Material of $Cu_{(1-2x)}Ni_{(x)}Zn_{(x)}Fe_2O_4$

Marziyeh Veisi [1], Yasser Rajabi [1], Ahmad Gholizadeh [1*]*

[1] *School of Physics, Damghan University, Damghan 36716-41167, Iran*

ARTICLE INFO

Article History:

Received 2024-11-02

Accepted 2025-12-31

Published 2024-05-05

Keywords:

Nano-magnetic materials;

spinel ferrite;

Jahn–Teller effect;

nonlinear optical properties;

diffraction ring patterns.

ABSTRACT

In this work, the nonlinear optical properties of $Cu_{(1-2x)}$ $Ni_{(x)}Zn_{(x)}Fe_2O_4$ nano-magnetic materials were systematically investigated in relation to the Jahn–Teller distortion degree. A series of samples with x = 0, 0.03, 0.06, and 0.09 were synthesized using the citrate method, where the co-substitution of Ni^{2+} and Zn^{2+} ions was employed to control the extent of Jahn–Teller distortion and induce a gradual structural transition from tetragonal to cubic symmetry. The nonlinear optical response of the prepared nanofluids was examined using the far-field diffraction ring patterns method under continuous-wave laser excitation at 532 nm. The evolution of diffraction rings was analyzed as a function of laser power and sample concentration, enabling the determination of the nonlinear refractive index (n_2) and thermo-optic coefficient (dn/dT). The results reveal a clear correlation between the Jahn–Teller distortion degree and the nonlinear optical behavior, where a reduction in structural distortion leads to a pronounced enhancement of the nonlinear response and diffraction ring formation. These findings demonstrate that the nonlinear optical properties of spinel ferrite nanofluids can be effectively tuned through Jahn–Teller distortion engineering, highlighting their potential for applications in optical switching, optical limiting, and photonic devices.

How to cite this article

Veisi M., Rajabi Y., Esmaeili A., Gholizadeh A., Harnessing the Jahn-Teller Effect for Enhanced Nonlinear Optical Properties in Nano-magnetic Material of $Cu_{(1-2x)}Ni_{(x)}Zn_{(x)}Fe_2O_4$. J. Nanoanalysis., 2024; 11(2): 686-702.

*Corresponding Author Email: y.rajabi@du.ac.ir; gholizadeh@du.ac.ir

INTRODUCTION

Nano-magnetic materials have attracted considerable attention due to their size-dependent physical properties and wide-ranging applications in data storage, magnetic sensors, biomedical devices, and photonic technologies [1–6]. At the nanoscale, subtle variations in crystal structure, cation distribution, and electronic configuration can significantly influence the optical and magnetic responses of these materials. In recent years, the integration of nano-magnetic materials into electro-optic and photonic systems has opened new opportunities for developing multifunctional devices with tunable optical characteristics [7–14].

Among nano-magnetic materials, spinel ferrites (MFe_2O_4) constitute an important class owing to their remarkable magnetic, electrical, and optical properties [15–18]. Their flexible crystal structure allows for various cation substitutions at tetrahedral and octahedral sites, enabling precise control over structural symmetry and electronic interactions. This tunability makes spinel ferrites promising candidates for nonlinear optical (NLO) applications, including optical modulation, optical limiting, and photonic switching [19–25]. Although nonlinear optical phenomena have been extensively investigated in semiconductors and dielectric materials, studies on spinel ferrite nanostructures remain relatively limited, particularly with respect to structure–property correlations.

One of the key structural factors influencing the physical properties of spinel ferrites is the Jahn–Teller effect (JTE), which originates from the presence of electronically degenerate states in transition-metal ions. In copper-containing ferrites, the Cu^{2+} ion with a $3d^9$ electronic configuration induces lattice distortion when occupying octahedral sites, leading to symmetry lowering from cubic to tetragonal structures [29–31]. This distortion alters the electronic band structure, orbital overlap, and phonon interactions, thereby affecting optical absorption, refractive index modulation, and nonlinear optical behavior. Closely related to the Jahn–Teller effect is the pseudo Jahn–Teller effect, which arises from vibronic coupling between non-degenerate electronic states and has been shown, through computational studies, to play a critical role in structural instability and electronic redistribution in various molecular and solid-state systems [32, 33]. Recent theoretical investigations have demonstrated that Jahn–Teller and pseudo Jahn–Teller interactions can significantly modify electronic energy landscapes and optical responses, emphasizing the importance of combining structural distortion analysis with electronic-level understanding.

Despite the recognized influence of the Jahn–Teller effect on the structural and magnetic properties of ferrites, its direct impact on nonlinear optical behavior, particularly in nano-magnetic fluids, has not been systematically explored. In most previous studies, nonlinear optical properties of ferrites were reported without explicitly correlating the observed optical response to controlled variations in Jahn–Teller distortion. Consequently, a clear experimental framework linking crystal symmetry distortion to nonlinear optical performance is still lacking.

In this work, we address this gap by systematically investigating the nonlinear optical properties of $Cu_{(1-2x)}\ Ni_{(x)}\ Zn_{(x)}\ Fe_2O_4$ nano-magnetic materials with controlled Jahn–Teller distortion degrees. By co-substituting Ni^{2+} and Zn^{2+} ions for Cu^{2+}, the extent of Jahn–Teller distortion is gradually reduced, inducing a structural transition from tetragonal to cubic symmetry. The nonlinear optical response of the resulting nanofluids is examined using the far-field diffraction ring patterns method under continuous-wave laser excitation. This technique provides a sensitive and direct probe

of nonlinear refractive effects, allowing the extraction of key parameters such as the nonlinear refractive index (n_2) and thermo-optic coefficient (dn/dT).

In this study, the nonlinear optical properties of $Cu_{(1-2x)}Ni_{(x)}Zn_{(x)}Fe_2O_4$ nano-magnetic materials are systematically investigated with an emphasis on the role of Jahn–Teller distortion. By co-substituting Ni^{2+} and Zn^{2+} ions for Cu^{2+}, the degree of Jahn–Teller distortion is deliberately tuned, leading to a gradual structural evolution from tetragonal to cubic symmetry. The nonlinear optical response of the resulting nanofluids is examined using the far-field diffraction ring patterns method under continuous-wave laser excitation, enabling the extraction of the nonlinear refractive index and thermo-optic coefficient. This approach establishes a direct experimental link between structural symmetry distortion and nonlinear optical behavior in spinel ferrite nanomaterials, demonstrating that Jahn–Teller distortion engineering provides an effective route for tuning nonlinear optical responses in ferrite-based systems.

EXPERIMENTAL

Materials

Copper nitrate ($Cu(NO_3)_2·3H_2O$), nickel nitrate ($Ni(NO_3)_2·6H_2O$), zinc nitrate ($Zn(NO_3)_2·6H_2O$), iron(III) nitrate ($Fe(NO_3)_3·9H_2O$), and citric acid ($C_6H_8O_7$) were used as starting materials for the synthesis of $Cu_{(1-2x)}Ni_{(x)}Zn_{(x)}Fe_2O_4$ nanoparticles. All chemicals were of analytical grade and were purchased from Merck (Germany) without further purification. Deionized water was used throughout the synthesis process.

Synthesis of $Cu_{(1-2x)}Ni_{(x)}Zn_{(x)}Fe_2O_4$ Nanomagnetic particles

$Cu_{(1-2x)}Ni_{(x)}Zn_{(x)}Fe_2O_4$ nanoparticles with x = 0, 0.03, 0.06, and 0.09 were synthesized using the citrate sol–gel method. Stoichiometric amounts of copper nitrate, iron(III) nitrate, nickel nitrate, and zinc nitrate were weighed according to the desired compositions (Table 1) and dissolved separately in deionized water to obtain clear solutions. Citric acid was then added as a chelating agent with a metal nitrate to citric acid molar ratio of 1:1.

The mixed solution was magnetically stirred at room temperature for 45 min to ensure homogeneity and subsequently heated in a water bath at 80 °C for 2.5 h under continuous stirring. During this process, ammonia solution was added dropwise to adjust the pH of the solution to approximately 7, which facilitated complex formation and gelation. The solution gradually transformed into a viscous gel upon continued heating.

The obtained gel was dried in an oven at 200 °C for 12 h with a controlled heating rate of 1 °C per 10 min to remove residual solvents and organic components. The resulting dried precursor was then calcined in air at temperatures of 450, 600, 750, and 900 °C to achieve phase formation and crystallization of the ferrite nanoparticles.

Table 1: The amount of grams calculated for each the composition $Cu_{(1-2x)}Ni_{(x)}Zn_{(x)}Fe_2O_4$

Result	x	$Cu(NO_3)_2$	$Ni(NO_3)_2$	$Fe(NO_3)_2$	$Zn(NO_3)_2$	$C_6H_8O_7$
$CuFe_2O_4$	0	1.0074	0	3.3775	0	6.4248
Cu0.94Ni0.03Zn0.03Fe2O4	0.03	0.9490	0.0364	3.3780	0.0328	6.4248
Cu0.88Ni0.06Zn0.06Fe2O4	0.06	0.8890	0.0730	3.3790	0.0656	6.4267
Cu0.82Ni0.09Zn0.09Fe2O4	0.09	0.8290	0.1090	3.3800	0.0980	6.4286

The Jahn-Teller effect

The Jahn-Teller effect (JTE) arises when a molecule in a degenerate electronic state distorts to lower its symmetry and energy. This phenomenon is common in transition metal complexes and affects their reactivity and magnetic properties. Understanding the Jahn-Teller effect is crucial in predicting and explaining the behavior of these systems in various chemical reactions and physical processes. Researchers continue to explore its intricacies and applications in diverse fields such as chemistry, physics, and materials sciences [30].

Among magnetic nano-materials, Spinel Magnetic Ferrites (SMF) has valuable optical, magnetic, and electrical properties [38]. The use of Spinel Ferrites has created a wide range of applications for them due to their magnetic and electrical properties such as high magnetization (Ms) and favorable dielectric properties. The structure of Spinel Ferrites can be represented by a general formula $(M_1 - \delta Fe\delta)[M\delta Fe_2 2 - \delta]O_4$, where δ is the inversion factor of the cation distribution. Also, M stands for a diva- lent metal ion (Mg^{2+}, Mn^{2+}, Co^{2+}, Ni^{2+}, Cu^{2+}, and Zn^{2+}). Fe is the trivalent metal cation (Fe^{3+}) occupies the FCC network formed by O^{2-} anions. Researchers employ the inversion parameter δ to assess the cation distribution in Spinel Ferrites. This parameter quantifies the degree of inversion between octahedral and tetrahedral sites within the crystal lattice. The larger the value of this parameter means that there are more the Jan Teller divalent cations ($Cu^{(2+)}$) in the octahedral position. The Jahn-Teller effect is caused by the presence of ($Cu^{(2+)}3d^9$) cations in the octahedral site, which leads to stretching or compressing the octahedral FeO_6 along the c-axis, and the spinel structure deviates towards tetragonal. Understanding the distribution of cations within spinel ferrites is essential for optimizing their magnetic and electrical properties [38]. By manipulating the inversion parameter, scientists can tailor these materials for specific applications in electronics, data storage, and other technological advancements. This research plays a key role in advancing material science and engineering disciplines.

Nonlinear optical setup

Various techniques to characterize the nonlinear (NL) optical response are presented. These methods include Z-scan technique[42], Pump-probe spectroscopy[43], Harmonic generation analysis[42], and Diffraction ring patterns analysis[39]. By employing these methods, researchers can better understand the nonlinear behavior of materials under intense laser irradiation, paving the way for innovative technologies in fields such as laser manufacturing, optical communications, and quantum optics. The Z-scan technique measures the nonlinear refractive index of a material by scanning a focused laser beam through it. Pump-probe spectroscopy involves the excitation of a sample with two synchronized laser pulses to study its ultrafast dynamics. Harmonic generation analysis studies the generation of higher harmonic frequencies in response to an incident laser beam. Diffraction ring patterns analysis involves analyzing the diffraction ring patterns formed when a material interacts with light. This advanced technique provides valuable insights into the nonlinear optical properties of materials and is important for various applications in photonics and optoelectronics. When a high-power Gaussian laser interacts with a non-linear medium, it produces far-field diffraction patterns known as Fraunhofer patterns. These patterns consist of concentric rings and their characteristics, such as the size of

the focal point and the spacing between the rings, vary based on the optical system's properties [39]. The formation of the ring pattern is a result of various physical mechanisms causing phase shifts on the Gaussian wave front [40]. Several physical mechanisms are responsible for the phase shift on the Gaussian wavefront that creates the shape of the rings in the Fraunhofer diffraction pattern. As a result, the distorted re-radiation waves have different frequencies from the incident wave, and from the number of loops, the relationship of the non-linear refractive index of the material is obtained. In the experimental setup (see figure 1), a Gaussian beam of a continuous-wave diode pumped solid state laser operating at a wavelength of 532 nm was directed at the cell using a lens with a focal length of 190 mm. The laser beam was carefully focused to ensure optimal illumination of the sample surface. The cell was placed between the lens and the focus point, containing nano-fluid had a path length of 1 mm. The setup also included a Camera (Basler acA640-750uc) to capture the interaction between the laser beam and the sample, providing valuable data on the sample's response to the laser irradiation. The Basler acA640-750uc USB 3.0 camera with the ON Semiconductor PYTHON, 300 CMOS sensor, delivers 751 frames per second at VGA resolution. The laser beam diameter at the sample was determined to be 0.5 mm. To ensure the effective heating of a fluid, the nano-fluid must exhibits a high absorption capacity for green light. Upon passing through the nano-fluid, the laser beam displayed a phenomenon of divergence, forming a series of concentric diffraction rings that illuminated the screen. The diffraction ring patterns were observed and documented by positioning the screen at a distance of 50 cm from the front of the cell.

RESULTS AND DISCUSSIONS

Characterization of $Cu_{(1-2x)}Ni_{(x)}Zn_{(x)}Fe_2O_4$ Nano-magnetic particles

Fig. 2 shows the X-ray diffraction patterns of $Cu_{(1-2x)}Ni_{(x)}Zn_{(x)}Fe_2O_4$ nanoparticles with different Jahn–Teller distortion degrees. The diffraction patterns indicate that increasing Ni/Zn co-substitution leads to a gradual structural transition from a tetragonal phase (x = 0) to a nearly cubic phase (x = 0.09). This transformation is attributed to the progressive reduction of Jahn–Teller distortion caused by the substitution of Cu^{2+} ions with Ni^{2+} and Zn^{2+} ions, which suppresses the cooperative Jahn–Teller effect associated with Cu^{2+} ($3d^9$) ions in octahedral sites. The observed phase evolution confirms that the Jahn–Teller distortion degree can be effectively controlled through compositional tuning.

Fig. 2 illustrates a gradual transition of the structural phase from tetragonal in sample $x = 0.0$ to nearly complete cubic in sample $x = 0.09$, indicating a complete Jahn-Teller effect transformation. Miller indices of the tetragonal and cubic structures, respectively, are labeled on the peaks of the X-ray diffraction patterns of samples $x = 0.0$ and $x = 0.09$, denoting the crystallographic phase changes.

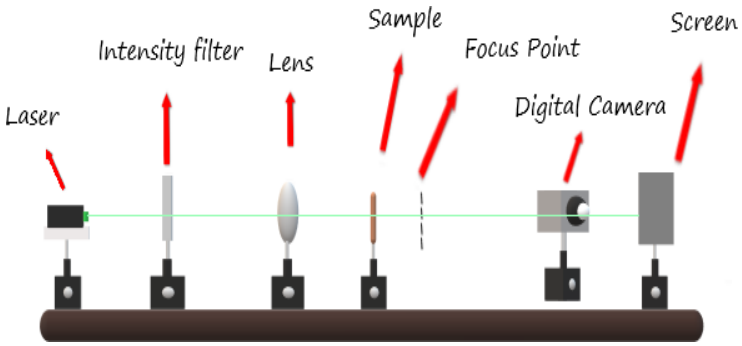

Fig. 1: Optical setup used to record the far-field diffraction ring patterns.

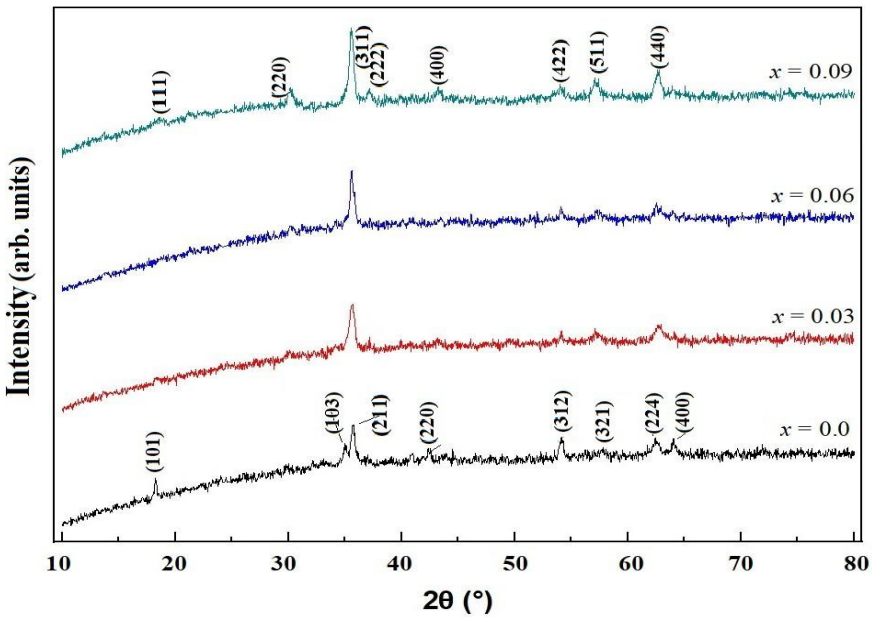

Fig. 2: 4: X-ray diffraction pattern of $Cu_{(1-2x)}\ Ni_{(x)}\ Zn_{(x)}\ Fe2O4$ with various the Jahn-Teller distortions.

Nonlinear optical studies

Our study has concentrated on exploring the correlation between the number of diffraction rings observed and the intensity of the excitation laser beams, the concentration of samples, and the Jahn-Teller degrees (x=0, 0.03, 0.06, and 0.09). By adjusting the power of the laser beam (p=147, 58, and 17.8 mW), we could observe variations in the diffraction pattern produced by the sample. Also, by changing the concentration of samples (c=0.01gr/cm^3, 0.03gr/cm^3, and 0.05gr/cm^3), the relationship between the number of diffraction rings and the concentration of nano-fluid determined. This analysis provided valuable insights into the material's response to different levels of laser irradiation and helped us characterize the optical properties of the sample under varying excitation conditions; the new results have led to calculating the nonlinear refractive index coefficient (n_2) and the thermo-optic coefficient (dn/dT). Fig. 3a-d shows the time evolution far-field diffraction patterns of the laser beam passing through the nano-fluid with the different Jahn-Teller distortion degree(x) in laser beam power of p=147 mW, which was recorded by increasing the input laser power. At

high input power ($p = 147mW$), with the increase of x, the Jahn-Teller effect (crystal disorder) decreases. As it is known, at $x = 0$ and $x = 0.03$, diffraction rings are not formed and have minimal resolution. At $x = 0.06$ and $x = 0.09$, the time evolution of the diffraction rings is quite evident. To investigate the dependence of the Jahn-Teller passing through the nano-fluid for (a) x=0, (b) x= 0.03, (c) x= 0.06, and x= 0.09.

Effect on the incident laser beam power on the sample, the complete diffraction rings are selected and shown in Fig. 4. This Fig. 4.a corresponds to the power of the incident laser beam equal to 147 mW, Fig. 4.b corresponds to the power of the incident laser beam equal to 58 mW, and Fig. 4.c corresponds to the laser beam with the incident power of 17.8 mW. Fig. 4, clearly shows that in power of 147 mW, shows nonlinear behavior more clearly compared to other powers (diffraction rings are obvious). It can also be seen at the power of 147 mW that more diffraction rings are observed with decreasing Jahn–Teller distortion degree, corresponding to higher Ni/Zn substitution levels. This behavior indicates that the reduction of Jahn–Teller-induced structural distortion enhances the nonlinear refractive response of the nanofluid. Also, with the rise of the power of the incident beam on the sample, the diffraction rings change from a circular shape (horizontal diameter equals vertical one) to an elliptical shape. When the diffraction rings change shape, it is a sign of increased convective effect in the vertical direction of each pattern, this phenomenon is called the collapse effect. In Fig. 4., it is pretty evident that with the increase of laser power, the convective effect has prevailed. In this effect, convection effect becomes relevant. The enhancement of diffraction ring formation at lower Jahn–Teller distortion degrees can be attributed to improved structural symmetry and reduced lattice strain, which facilitate stronger light–matter interaction and more efficient nonlinear refractive index modulation.

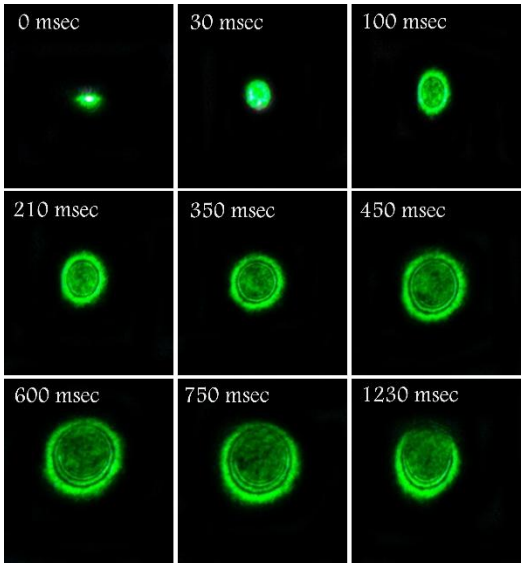

(a)

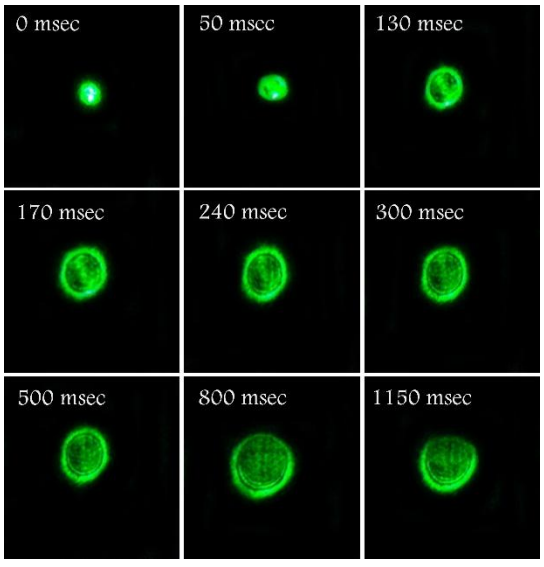

(b)

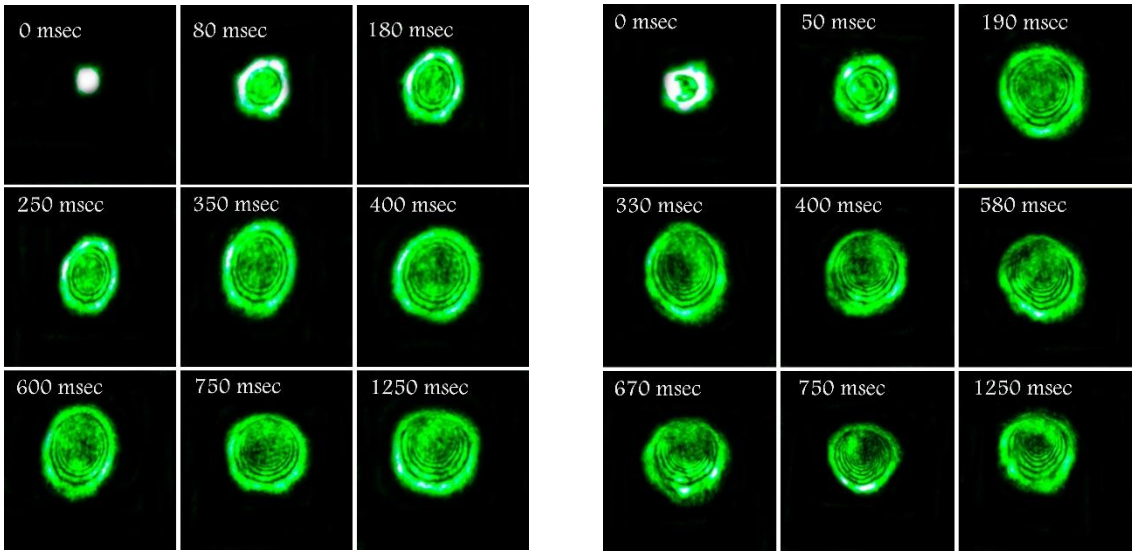

(c) (d)

Fig. 3: Images of the temporal evolution of the far-field diffraction pattern of a 147 mW laser beam

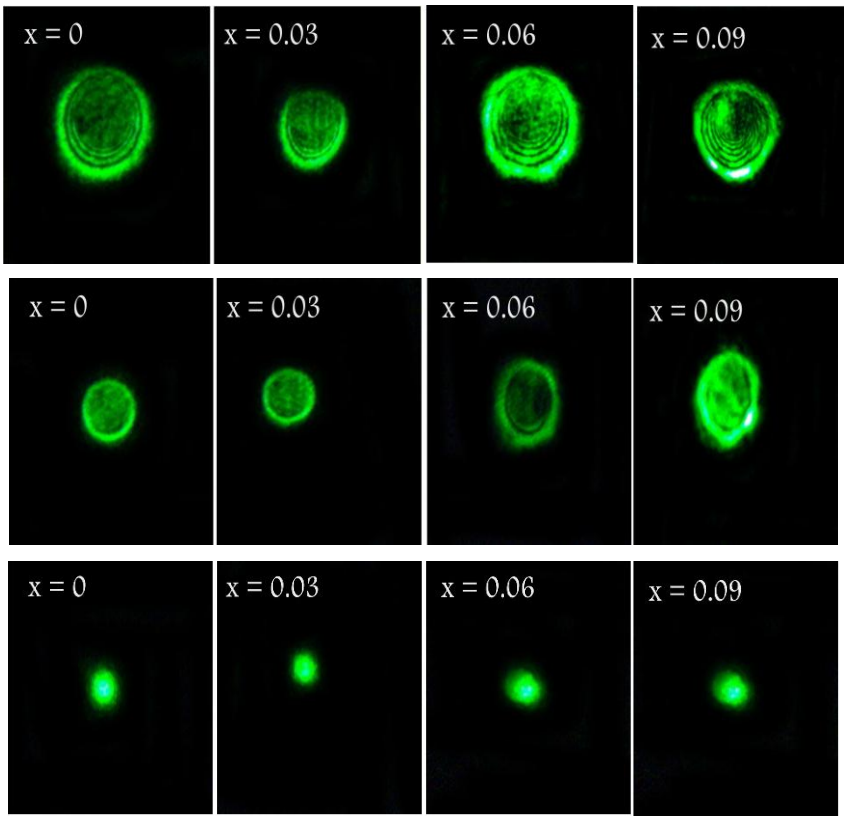

(a)

(b)

(c)

Fig. 4: The observed diffraction rings with different the Jahn-Teller distortion degree at far field on screen with different laser beam powers (a)147mW, (b)58mW, and (c) 17.8mW.

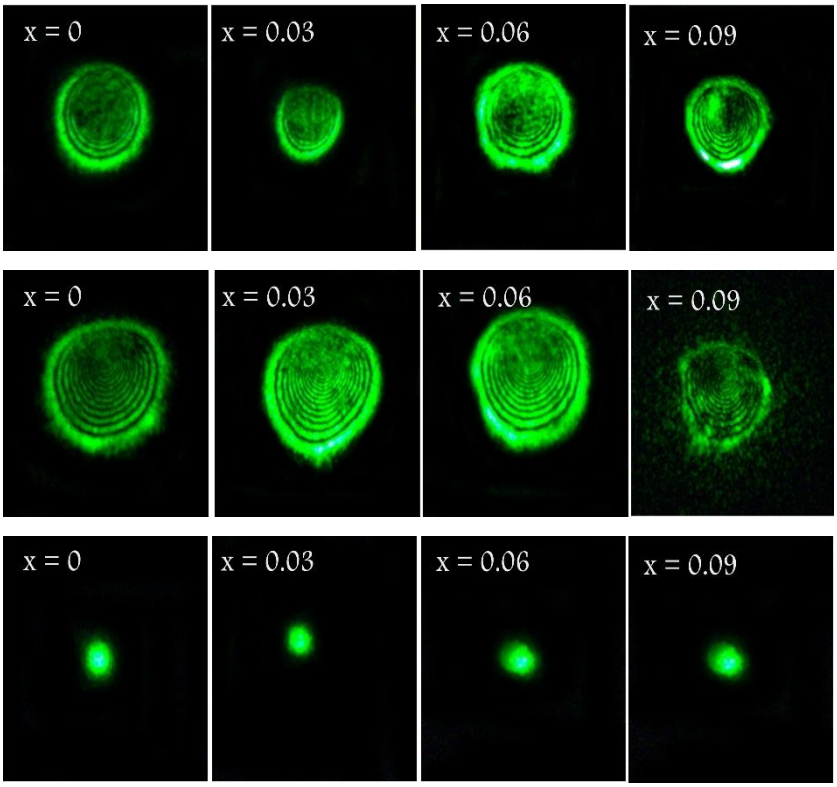

Fig. 5: The observed diffraction rings with different the Jahn-Teller distortion degree at far field on screen in power 147mW with different concentrations (a)0.01gr/cm^3, (b)0.03gr/cm^3, and (c) 0.05 gr/cm^3.

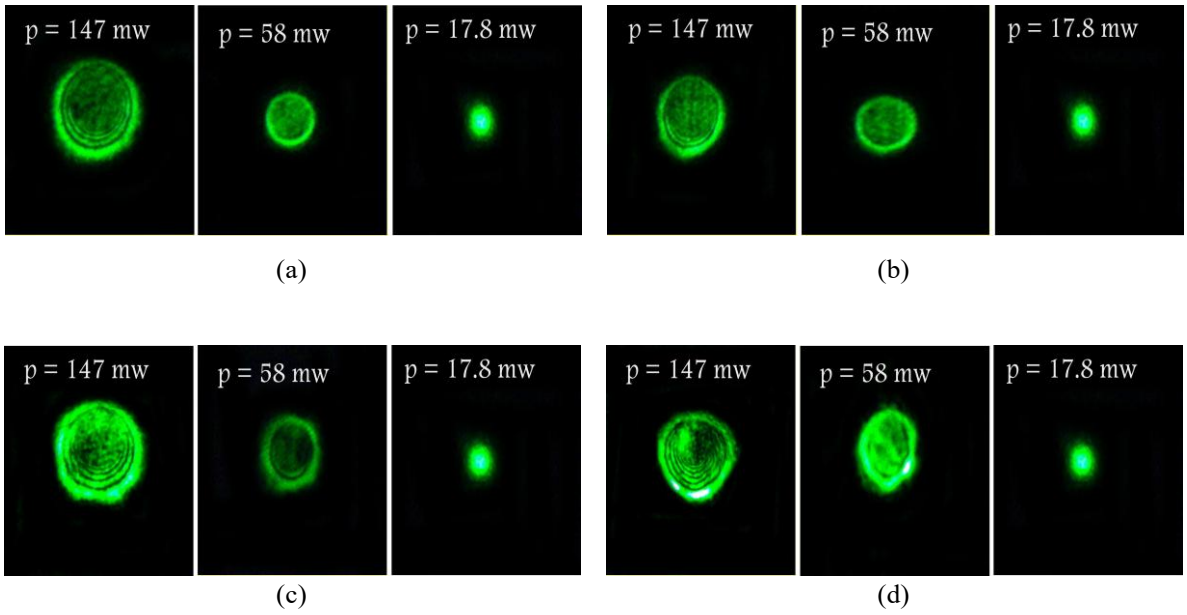

Fig. 6: The observed diffraction rings with different input laser power and with the Jahn-Teller distortion degrees (a) x=0, (b) x= 0.03, (c) x = 0.06, and (d) x=0.09.

Fig. 5, clearly shows that in C=0.03gr./cm^3, shows nonlinear behavior more clearly compared to other concentrations (diffraction rings are completely visible).

In Fig.6, it is clear that in 147mW and x= 0.09, the diffraction rings pattern deformed. This shows that the collapse effect starts to appear in the nano-magneto fluid.

Fig. 7, shows the changes in the nonlinear behavior of the samples at different concentrations. Fig. 7 clearly shows that as the concentration of nano-fluid increases, the number of diffraction rings increases, and also, the shape of the rings changes. In concentrations of 0.01gr/cm^3 and 0.03gr/cm^3, the rings are completely circular (horizontal and vertical diameters are equal). In this concentration, conduction effects are dominant and convection effects are negligible. At a higher concentration, i.e. c= 0.05gr/cm^3, the shape of the diffraction rings changes, and the vertical diameter increases compared to the horizontal diameter. In this concentration, the effect of convective flow becomes dominant. In Fig. 7. b and c correspond to x=0.03 and 0.06, results show that in the concentration of c=0.03 gr/cm^3 and 0.05 gr/cm^3 the shape of the diffraction rings changes. This result clearly shows that with the decrease in the Jahn-Teller effect distortion degree, the deformation of the diffraction rings has increased, and in fact, the dominance of the convective effect has increased.

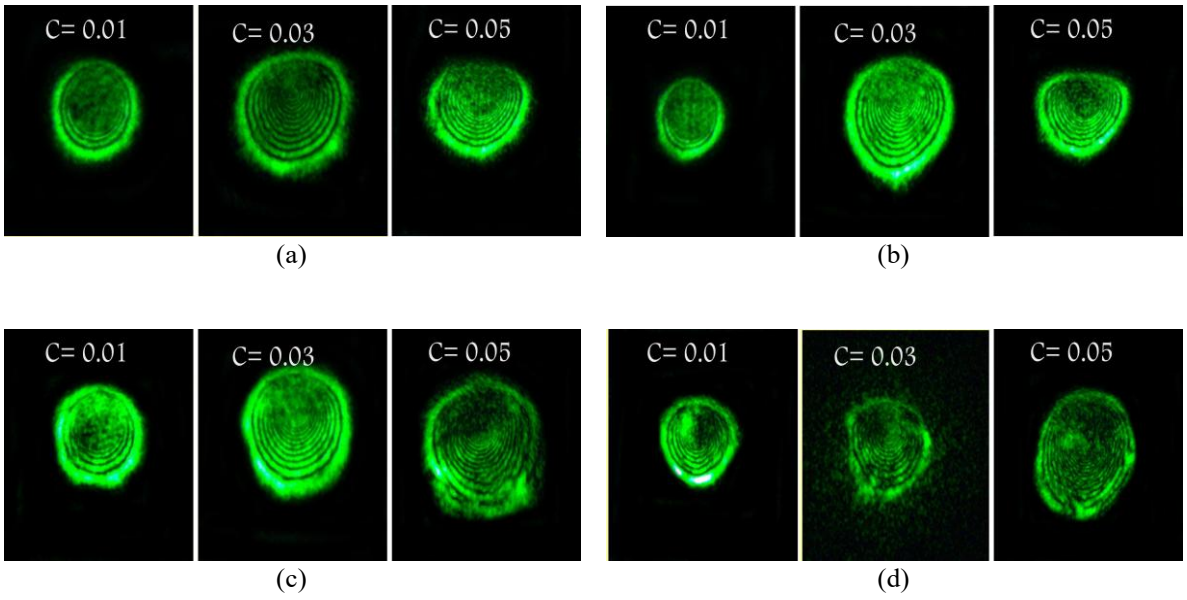

Fig. 7: The observed diffraction rings with different concentrations of samples and with the Jahn-Teller distortion degrees (a) x=0, (b) x= 0.03, (c) x=0.06, and (d) x = 0.09.

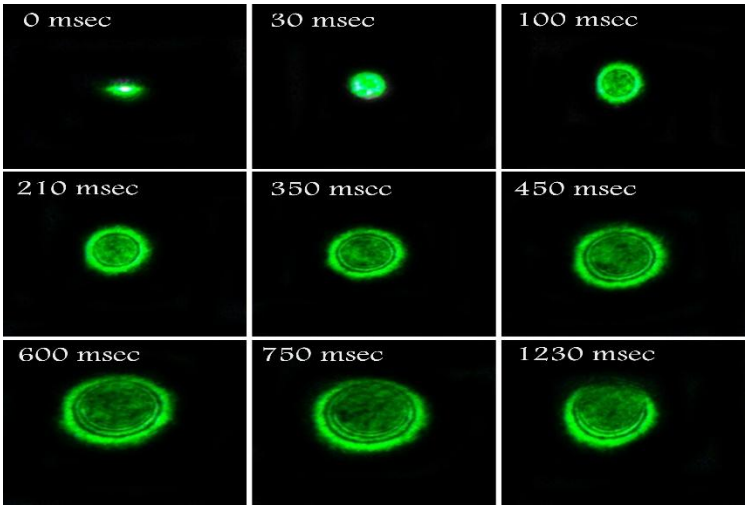

(a)

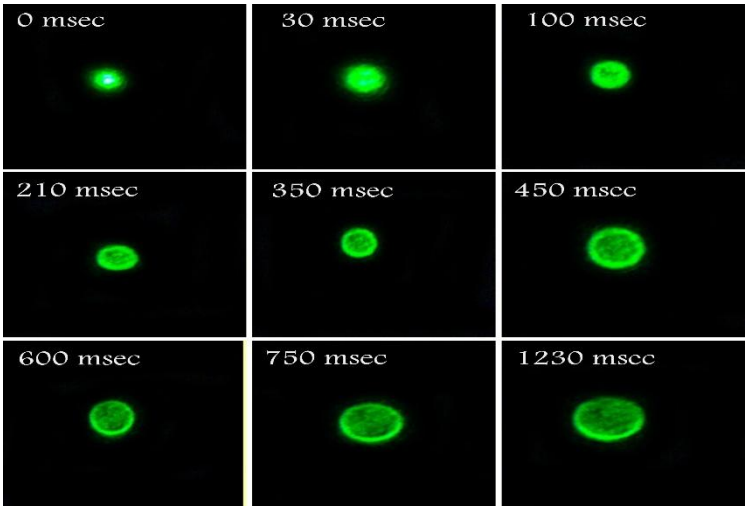

(b)

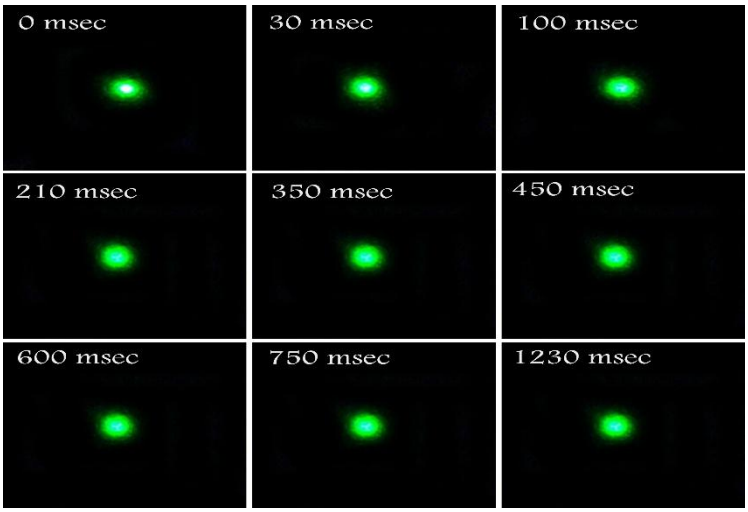

(c)

Fig. 8: Images of the temporal evolution of the far-field diffraction pattern of a laser beam passing through the liquid sample for x=0, and (a) p=147mW, (b) p= 58mW, and (c) p=17.8mW.

Table 2: The calculated NL optical parameters. N/A indicates that diffraction rings were not clearly formed and the nonlinear refractive index could not be reliably extracted.

	$n_2(cm^2/W) \times 10^{-12}$						
	$P_1 = 147mW$			$P_2 = 58mW$			$P_3 = 17.8mW$
	$C_1 = 0.01$	$C_2 = 0.03$	$C_3 = 0.05$	$C_1 = 0.01$	$C_2 = 0.03$	$C_3 = 0.05$	$C_{1,2,3}$
x = 0	−0.8736	−2.1840	−1.9656	−0.5535	−2.7677	−1.6606	N/A
x = 0.03	−0.6552	−2.6208	−2.1840	−0.5535	−3.3213	−2.2142	N/A
x = 0.06	−1.0920	−3.0577	−2.4024	−0.5535	−3.3213	−2.2142	N/A
x = 0.09	−1.3104	−3.4945	−2.6208	−0.5535	−4.4284	−2.7679	N/A

Fig. 8a-c shows the temporal evolution far-field diffraction patterns of the laser beam passing through the nano-fluid with lower Jahn-Teller distortion degree ($x = 0$) in different concentration of nano-fluid in high power laser (147mW). The diffraction rings were recorded by changing the concentration of samples. The change in the non-linear behavior of the sample is observed in different concentrations. In Fig. 8 observed that, because conductive effects prevail over convective effects in the nano-fluid, the spot of the laser beam remains circular (vertical diameter equals the horizontal one) until about 300 *ms*. But deformed the spot diffraction rings after about 450 ms, the convective effects become relevant. The diameter of the outermost ring in the vertical direction increases with the increasing the time of laser radiation, after 700 ms in the horizontal direction the diameter of the outermost ring increases with the increasing the time of laser radiation.

The intensity-dependent refractive index is given by [43]

$$n = n_0 + n_2 I \quad (1)$$

Where n_2 is the nonlinear refractive index or the third-order refractive index, I is laser input intensity ($I = \frac{2p_2}{\pi\omega_0}$), n_0 is the linear refractive index, and n is the total refractive index of the medium. Also, the nonlinear refractive index can be expressed in term $X^{(3)}$:

$$n_2 = \frac{3ReX^{(3)}}{4\epsilon cn^2} \quad (2)$$

The nonlinear refractive index n_2 for the diffraction ring patterns can be expressed by following equation [39]:

$$n_2 = \frac{\pi\omega_0^2\lambda N}{2L_{eff}P'} \quad (3)$$

Where the Eq. 3 The nonlinear refractive index (n_2) is related to the number of rings observed (N), ω_0 is the beam waist of the laser beam in a focal point, and L_{eff} effective length.

The captured observed diffraction rings were accounted for from the obtained figures. Then, all the nonlinear refractive indices (n_2) are obtained by using Eq. 3. Its calculated values for n_2 are shown in Table 2.

The comparison of the number of diffraction rings with the Jahn-Teller distortion degree in laser power intensity of 147mW is illustrated in Fig. 9a, where a clear correlation is observed. Conversely, Fig. 9b presents the association between these factors in various sample concentrations. Notably, at C = 0.03gr/cm^3, significant enhancements in the sample's nonlinear characteristics were identified. This finding suggests a direct link between the Jahn-Teller effect and the optical behavior of the material.

The relation between the number of diffraction rings and laser power intensity is illustrated in Fig. 10. The straight red line denotes the fitting of experimental data to $x = 0$ (highest

the Jahn-Teller distortion). The slope of the highest of the Jahn Teller distortion is the most significant value among other samples ($\frac{dN}{dP} = 0.1053$). This graphical representation provides a clear visualization of how the diffraction rings change in response to varying laser power intensities. Understanding this relationship is crucial for interpreting the experimental results accurately and drawing meaningful conclusions about the nonlinear optical behavior of nano-magnetic materials. Overall, the nonlinear optical measurements demonstrate a strong correlation between Jahn–Teller distortion degree and nonlinear refractive behavior in $Cu_{(1-2x)}\ Ni_{(x)}\ Zn_{(x)}\ Fe2O4$ nano-fluids. The systematic reduction of Jahn–Teller distortion enhances diffraction ring formation and nonlinear refractive index magnitude, highlighting the critical role of structural symmetry in governing nonlinear optical responses.

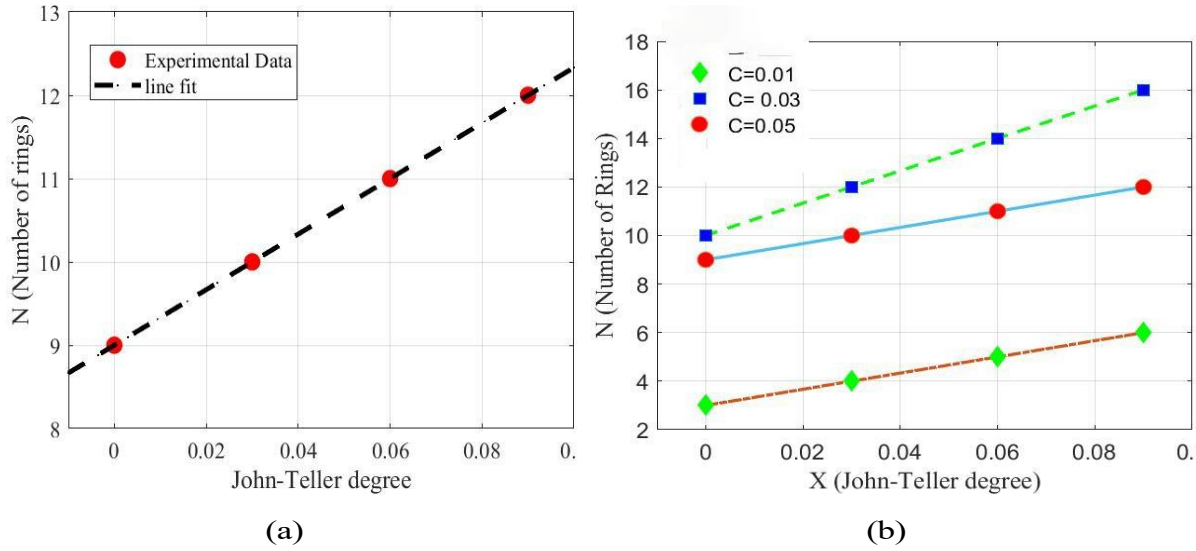

Fig. 9: Variation of the No. Of diffraction rings concerning to the Jahn-Teller distortion degree in (a) power laser=147mW, and (b) different concentrations

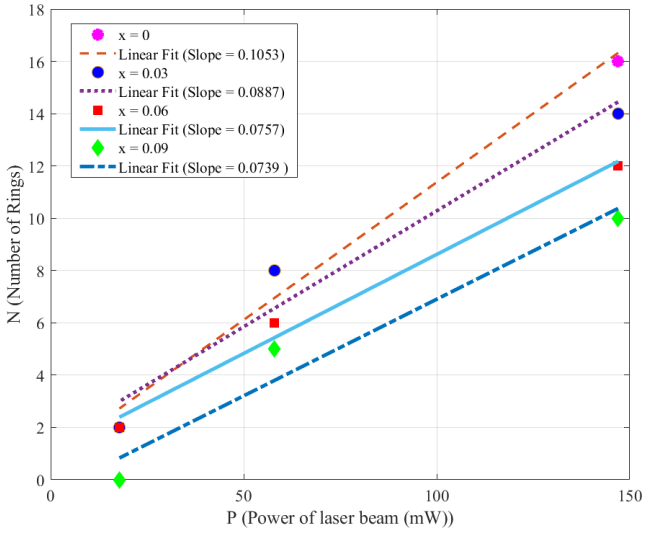

Fig. 10: Variation of the No. Of diffraction rings concerning the incident laser power intensity.

CONCLUSION

In this study, Cu (1−2x) Ni(x) Zn(x) Fe_2O_4 nano-magnetic materials with different Jahn–Teller distortion degrees were successfully synthesized using the citrate method. Controlled co-substitution of Ni^{2+} and Zn^{2+} ions for Cu^{2+} enabled systematic tuning of the Jahn–Teller distortion, resulting in a gradual structural transition from tetragonal to cubic symmetry. The nonlinear optical behavior of the resulting nanofluids was investigated using the far-field diffraction ring patterns technique under continuous-wave laser excitation.

The experimental results demonstrate a clear and direct correlation between Jahn–Teller distortion and nonlinear optical response. A reduction in Jahn–Teller induced structural distortion leads to enhanced diffraction ring formation and an increased nonlinear refractive index, indicating stronger light–matter interaction in samples with higher structural symmetry. The observed dependence of nonlinear optical parameters on laser power and sample concentration further confirms the sensitivity of the nonlinear response to both intrinsic structural factors and external excitation conditions.

Overall, these findings establish Jahn–Teller distortion engineering as an effective strategy for tuning the nonlinear optical properties of spinel ferrite nanofluids. By linking crystal symmetry control to nonlinear optical performance, this work provides valuable insights into the design of nano-magnetic materials for photonic and optoelectronic applications.

Outlook and Future Perspectives

Future studies could benefit from complementary theoretical and computational investigations, such as density functional theory or ligand-field-based modeling, to further elucidate the electronic mechanisms underlying Jahn–Teller and pseudo Jahn–Teller effects in ferrite systems. Extending the present approach to other dopant combinations, excitation wavelengths, and experimental configurations may enable enhanced control over nonlinear optical behavior. Moreover, exploring practical device-level demonstrations, including optical limiting and all-optical switching applications, could further advance the technological potential of Jahn–Teller-engineered nano-magnetic materials.

REFERENCES

[1]. Taghizadeh, M., Bozorgzadeh, F., Ghorbani, M. Designing magnetic field sensor based on tapered photonic crystal fiber assisted by a ferrofluid. Sci Rep 11, 14325, https://doi.org/10.1038/s41598-021-93568-z (2021).

[2]. Sharma, A. K., Popescu, V. Magnetic field sensor with truncated honeycomb pho- tonic crystal fiber: analysis under the variations in magnetic fluid composition and temperature for high performance in near infrared. Opti. Quantum Electron. 53, 145. https://doi.org/10.1007/s11082-021-02795-1 (2021).

[3]. Nemala, H. et al. Investigation of magnetic properties of fe3o4 nanoparticles using temperature dependent magnetic hyperthermia in ferrofluids. J. Appli. Phys. 116, 034309. https://doi.org/10.1063/1.4890456 (2014).

[4]. Luo, X.; Al-Antaki, A. H. M.; Alharbi, T. M. D.; Hutchison, W. D.; Zou, Y.-c.; Zou, J.;

Antony, S.; Zhang, W.; Raston, C. L. Laser-Ablated Vortex Fluidic-Mediated Synthesis of Superparamagnetic Magnetite Nanoparticles in Water Under Flow. ACS Omega. 3, 11172? 11178, https://doi.org/10.1021/acsomega.8b01606 (2018)

[5]. Mohamed, N., Moaied, M. Enhancement of electronic and magnetic properties in Cr2O3 monolayer honeycomb-kagome by hydrogenation and oxygenation. Eur. Phys. J. Plus 138, 1075, https://doi.org/10.1140/epjp/s13360-023-04728-1 (2023).

[6]. Hu, Y., Yu, M., Buscaino, B. et al. High-efficiency and broadband on- chip electro-optic frequency comb generators. Nat. Photon. 16, 679?685, https://doi.org/10.1038/s41566-022-01059-y (2022)

[7]. Qin, Jun, Xia, Shuang, Yang, Weihao, Wang, Hanbing, Yan, Wei, Yang, Yucong, Wei, Zixuan, Liu, Wenen, Luo, Yi, Deng, Longjiang and Bi, Lei. ”Nanophotonic devices based on magneto-optical materials: recent developments and applica- tions” Nanophotonics, 11, 11, 2639-2659,https://doi.org/10.1515/nanoph-2021-0719 (2022)

[8]. M. Abutalib, A. Rajeh, Influence of Fe3O4 nanoparticles on the optical, magnetic and electrical properties of PMMA/PEO composites: Combined FT-IR/DFT for electrochemical applications, Journal of Organometallic Chemistry, 920, 121348, https://doi.org/10.1016/j.jorganchem.2020.121348 (2020)

[9]. B. G. Ghamsari, P. Berini, Nonlinear optics rules magnetism, Nature Photonics, 10, 74?75, 2016.

[10]. T. Morimoto, N. Nagaosa, Topological nature of nonlinear optical effects in solids, Science Advances, 2, 5, 1501524, 2016.

[11]. Junchao Ma, Qiangqiang Gu, Yinan Liu, Jiawei Lai, Peng Yu, Xiao Zhuo, Zheng Liu, Jian-Hao Chen, Ji Feng, Dong Sun, Nonlinear photoresponse of type-II Weyl semimetals, Nature Materials, 18, 476?481, 2019.

[12]. Shoufeng Lan, Lei Kang, David T. Schoen, Sean P. Rodrigues, Yonghao Cui, Mark L. Brongersma, Wenshan Cai, Backward phase-matching for nonlinear optical generation in negative-index materials, Nature Materials, 14, 807?811, 2015.

[13]. Yuting Ye, Yuehui Xian, Jiawen Cai, Kaicheng Lu, Zhengzheng Liu, Tongchao Shi, Juan Du, Yuxin Leng, Rongfei Wei, Weiqi Wang, Xiaofeng Liu, Gang Bi, Jian-rong Qiu, Linear and Nonlinear Optical Properties of Few?Layer Exfoliated SnSe Nanosheets, Advanced Optical Materials, 7, 5, 2019.

A. Handelman, S. Lavrov, A. Kudryavtsev, A. Khatchatouriants, Y. Rosenberg, E. Mishina, G. Rosenman, Nonlinear Optical Bioinspired Peptide Nanostructures, 1, 11, 2013.

[14]. Agus Rimus Liandi, Antonius Herry Cahyana, Ahmad Jauhari Fadillah Kusumah, Ardita Lupitasari, Diva Naufal Alfariza, Rahma Nuraini, Renita Wulan Sari, Findi Citra Kusumasari, Recent trends of spinel ferrites (MFe2O4: Mn, Co, Ni, Cu, Zn) applications as an environmentally friendly catalyst in multicomponent reactions: A review, Case Studies in Chemical and Environmental Engineering, 7, 100303, https://doi.org/10.1016/j.cscee.2023.100303, (2023).

[15]. Sandeep Kumar Singh, Yaswanth K.

Penke, J. Ramkumar, M.J. Akhtar, Kamal K. Kar, Facile synthesis of Al substituted Cu-ferrite infused reduced graphene oxide (rGO) nanohybrid for improving microwave absorption at gigahertz frequencies, Journal of Alloys and Compounds, 901, 163659, https://doi.org/10.1016/j.jallcom.2022.163659 , (2022).

[16]. Ali Alizadeh, Yasser Rajabi, M.M. Bagheri?Mohagheghi, Effect of crystallinity on the nonlinear optical properties of indium?tin oxide thin films, Optical Materials, 131, 2022, 112589, ISSN 0925-3467, https://doi.org/10.1016/j.optmat.2022.112589.

[17]. Rajabi, Y., Adelifard, M., Darabi, H. Nonlinear Optical Properties of Triple Thin Film FTO/SiO/GO, rGO. J. Electron. Mater. 52, 4940?4950, https://doi.org/10.1007/s11664-023-10430-w (2023).

[18]. K. O. Brien, H. Suchowski, J. Rho, A. Salandrino, B. Kante, X. Yin, Xiang Zhang, Predicting nonlinear properties of metamaterials from the linear response, Nature Materials, 14, 379?383, 2015.

[19]. Seung?Chul. Lee, Bong Joo Kang, Min?Jeong Koo, Seung?Heon Lee, Jae?Hyun Han, Jae?Young Choi, Won Tae Kim, Mojca Jazbinsek, Hoseop Yun, Dongwook Kim, Fabian Rotermund, O?Pil Kwon, Nonlinear Optics: New Electro?Optic Salt Crystals for Efficient Terahertz Wave Generation by Direct Pumping at Ti:Sapphire Wavelength, Advanced Optical Materials, 5, 2017.

[20]. F. Timpu, M. Reig Escale, M. Timofeeva, N. Strkalj, M. Trassin, M. Fiebig, and R. Grange, Enhanced Nonlinear Yield from Barium Titanate Metasurface Down to the Near Ultraviolet, Advanced Optical Materials, 2019.

[21]. Sijo S. Thomas, I. Hubert Joe, P. Aswathy, Elizabeth Mathew, A. Alice Noble, Structural, magnetic, and nonlinear optical properties of calcium doped Ni-Zn fer- rite nanoparticles synthesized by co-precipitation method, Materials Science and Engineering: B, 297, , 116696, https://doi.org/10.1016/j.mseb.2023.116696, (2023)

[22]. A.M.A. Henaish, B.I. Salem, T.M. Meaz, Yamen A. Alibwaini, Abdul-Wali Ajlouni, O.M. Hemeda, Enas A. Arrasheed, Synthesize, characterization, dielec- tric, linear and nonlinear optical properties of Ni?Al Ferrite/PANI nanocomposite film, Optical Materials, 119, 111397, https://doi.org/10.1016/j.optmat.2021.111397,(2021)

[23]. Helayl, S., Hassab-Elnaby, S., Badr, Y. et al. Nonlinear optical absorption and optical limiting of magnetic iron oxide nanomaterials. SN Appl. Sci. 5, 229, https://doi.org/10.1007/s42452-023-05449-x, (2023).

[24]. Asal Nowrouzi Gheymasi, Yasser Rajabi, Ehsan Nazarzadeh Zare, Nonlinear opti- cal properties of poly(aniline-co-pyrrole)@ ZnO-based nanofluid, Optical Materials, 102, 109835, 0925-3467, https://doi.org/10.1016/j.optmat.2020.109835, (2020)

[25]. B. Stern, X. Ji, Y. Okawachi, A. L. Gaeta, and M. Lipson, Battery-operated integrated frequency comb generator, Nature, 562, 401?405, 2018.

[26]. S. Keren-Zur, T. Ellenbogen, A new dimension for nonlinear photonic crystals, Nature Photonics, 12, 575?577, 2018.

[27]. S. D. Smith, Laser, nonlinear optics and optical computers, Nature, 316, 1985.

[28]. Wang, S., Khan, A.A., Teale, S. et al.

Large piezoelectric response in a Jahn-Teller distorted molecular metal halide. Nat Commun 14, 1852, https://doi.org/10.1038/s41467-023-37471-3, (2023).

[29]. Li, M., Zhang, M., Vendrell, O. et al. Ultrafast imaging of spontaneous sym- metry breaking in a photoionized molecular system. Nat Commun 12, 4233, https://doi.org/10.1038/s41467-021-24309-z (2021).

[30]. Klupp, G., Matus, P., Kamaras, K. et al. Dynamic Jahn?Teller effect in the parent insulating state of the molecular superconductor Cs3C60. Nat Commun 3, 912, https://doi.org/10.1038/ncomms1910 (2012).

[31]. Esmaili, A., Pseudo Jahn–Teller Effect in Si_4X_4 (X = F, Cl, Br, I) molecules: A theoretical investigation, Molecular Physics, 2019, 117, 567–574.

[32]. Mahmoudzadeh, G., Ghiasi, R., Pasdar, H., Computational investigation of the Pseudo Jahn–Teller effect on the structure and chemical properties of perhaloethene anions, Journal of Structural Chemistry, 2019, 60, 736–745.

[33]. R. Udayabhaskar, Muhamed Shafi Ollakkan, and B. Karthikeyan, Preparation, optical and non-linear optical power limiting properties of Cu, CuNi nanowires, Appl. Phys. Lett. 104, 013107, 2014.

A. Sommer, E. M. Bothschafter, S. A. Sato, C. Jakubeit, T. Latka, O. Razska- zovskaya, H. Fattahi, M. Jobst, W. Schweinberger, V. Shirvanyan, V. S. Yakovlev, R. Kienberger, K. Yabana, N. Karpowicz, M. Schultze and F. Krausz, Attosec- ond nonlinear polarization and light?matter energy transfer in solids, Nature, 534, 86?90, 2016.

[34]. Wenlong Hu Yikai Chen Hao Jiang Jingguo Li Gang Zou Qijin Zhang Douguo Zhang Pei Wang Hai Ming , Optical Waveguide Based on a Polarized Polydiacety- lene Microtube, 26,19, 2014.

[35]. S. Abed, K. Bouchouit, M. S. Aida, S. Taboukhatd, Z. Sofiani, B. Kulyk, V.Figa, Nonlinear optical properties of zinc oxide doped bismuth thin films using Z-scan technique, Optical Materials, 56, 40-44, 2016.

[36]. Correlation between structural phase transition and physical properties of Co2+/Gd3+ co-substituted copper ferrite, 2023.

[37]. R. Karimzadeh, Studies of spatial self-phase modulation of the laser beam passing through the liquids, Optics Communications, 286, 2013.

[38]. Elias RS, Hassan QMA, Emshary CA, Sultan HA, Saeed BA. Formation and temporal evolution of diffraction ring patterns in a newly prepared dihydropyridone. Spectrochim Acta A Mol Biomol Spectrosc. 2019.

[39]. M. Sheik-bahae, A. A. Said, E. W. Van Stryland, High-sensitivity, single-beam n_2 measurements. Opt. Lett. 14, 17, 955?957, 1989.

[40]. Luca Bolzonello, Matteo Bruschi, Barbara Fresch, and Niek F. van Hulst, Non- linear Optical Spectroscopy of Molecular Assemblies: What Is Gained and Lost in Action Detection, J. Phys. Chem. Lett. 2023, 14, 50, 11438?11446.

[41]. R. Boyd, Nonlinear Optics, 3rd Edition, ISBN: 9780080485966, Academic Press, 1-640, 2008.